



Comparison of the Coronal Green-line Intensities with the EUV Measurements from SDO/AIA

Xue-Fei Zhang^{1,2}, Yu Liu^{1,2,3,4,5,6}, Ming-Yu Zhao¹, Ji-Hong Liu^{1,3}, Abouazza Elmhamdi⁵, Teng-Fei Song^{1,2}, Zi-Han Li^{1,6}, Hong-Bo Li⁷, Fei-Yang Sha^{1,2} , Jing-Xing Wang¹, Xiao-Bo Li¹, Yuan-Deng Shen^{1,2}, Shun-Qing Liu¹, Hong-Fei Liang⁶, and R. M. Al-Shammari⁵

¹ Yunnan Observatories, Chinese Academy of Sciences, Kunming 650011, China; lyu@yao.ac.cn, zhangxuefei@yao.ac.cn

² University of Chinese Academy of Sciences, Beijing 100049, China

³ Shijiazhuang University, Shijiazhuang 050035, China

⁴ School of Physical Science and Technology, Southwest Jiaotong University, Chengdu 610031, China

⁵ Department of Physics and Astronomy, King Saud University, P.O. Box 2455, Riyadh 11451, Saudi Arabia

⁶ Yunnan Normal University, School of Physics and Electronic Information, Kunming 650500, China

⁷ Institute of Space Physics, Luoyang Normal University, Luoyang 471934, China

Received 2022 March 19; revised 2022 May 10; accepted 2022 May 12; published 2022 June 14

Abstract

The intensity of the green line (Fe XIV 5303 Å) is the strongest in the visible spectrum of the solar corona, and this line has been used as long-term powerful diagnostic tools for studying the coronal configurations and hot plasma dynamics. However, it remains unclear and an open question whether there exists close relationship between the green line intensities and the coronal extreme ultraviolet (EUV) line emissions for various coronal structures. In this paper, we use the green-line data by the Lijiang YOGIS Lyot coronagraph and the EUV data from the Solar Dynamics Observatory/Atmospheric Imaging Assembly instruments in order to perform direct comparisons and analyses, based on two algorithms developed to extract particular features in the low corona. It is found that, among the correlation coefficients obtained between the intensities of 5303 Å and the EUV lines, the coefficients between the green line and the 211 Å wavelength for different coronal structures and different limb locations always keep the highest values (ranging from 0.89 to 0.99), which has not been reported before. This result can be helpful and promising to link together the various physical processes involved at different heights in the corona by precisely tracking the bright loops or other features observed in 5303 Å above the limb down to the correct surface locations revealed by the 211 Å data. Furthermore, the ground-based observations of the coronal green line and the space-based EUV observations at 211 Å can advantageously complement each other when there is a need.

Key words: Sun: corona – Sun: magnetic fields – stars: coronae

1. Introduction

The solar corona is made up with highly ionized, low-density, hot plasma with temperature of million degrees. The well-known coronal green line (5303 Å) is formed by the forbidden transitional process (${}^2P_{3/2} - {}^2P_{1/2}$) in the $3s^23p$ ground configuration of the ion of Fe XIV. The green line emission was first discovered from solar eclipse observations (Young 1870), and has been extensively used for the regular observations by coronagraphs. Its high formation temperature and brightness make it a useful spectral line for diagnosing hot coronal structures (Grotrian 1934; Edlén & Swings 1942; Arnaud 1982; Stix 2004; Srivastava et al. 2007; Raju et al. 2011). It was Bernard Lyot who invented the coronagraph and successfully carried out the first off-eclipse observation from a mountain (Lyot 1939). For achieving direct coronal observations in optical wavelengths at a site, the sky background brightness is a critical site parameter which is required to be as low as possible. Several early coronagraph stations had been

constructed on high mountains for gaining the advantage of low scattered light level. The long-term regular coronal observations had been initiated at Pic du Midi, Climax, Arosa, Wendelstein, Kanzelhöhe, Norikura and Sacramento Peak et al. (Sakurai 2012). Currently, the observations of the coronal green line are continuously conducted mainly at three ground-based stations: Lomnický štít of Slovakia (Sakurai et al. 2004), Kislovodsk of Russia (Gnevyshev et al. 1967) and Lijiang of China (Liu & Zhang 2018). The operation of the Lijiang 10 cm coronagraph was based on the collaboration with the Norikura Station of NAOJ since 2013 (Zhang et al. 2022).

By using the coronal green line observations together with the other multi-wavelength data, parameters like plasma density, temperature, velocity, magnetic field and other information could be deduced and subsequently exploited for coronal physics studies. For example, the variations of the coronal temperature, through investigating the long-term observations of the coronal green line and the red line, indicate

the possible connection of a decrease of coronal temperature due to an increase of the area of polar coronal holes (Makarov et al. 2003). The coronal activities, such as solar flares, coronal bright points and coronal waves, are believed to be associated with the underlying magnetic fields (Sakurai et al. 2002; Shen & Liu 2012; Tian et al. 2012). The high-resolution measurements of the coronal green line corresponding to any scale of activities on the solar disk could be a good diagnostic tool for clearing the problems of coronal heating and solar wind acceleration (e.g., Smartt et al. 1993; Wood et al. 1998; Doschek et al. 2001; Minarovjech et al. 2003; Koutchmy et al. 2005; Ji et al. 2012, 2021; Yang et al. 2015; Dai et al. 2021). Statistically, the coronal green line intensity distributions and variations were found to be highly associated with large scale magnetic fields on the photosphere, and their evolution as a function of position angle along the solar limb were used to study solar cycles (Sýkora 1969; Guhathakurta & Fisher 1994; Deng et al. 2012; Antonucci et al. 2020). Although the coronal green-line enhanced features always occur at the locations of sunspots and plages with strong magnetic fields, the peak intensity does not depend on the strength of the underlying magnetic field (Ramesh et al. 1999). Petrovay et al. (2018) report that the forthcoming solar maximum will occur in 2024 October based on the data of the coronal green line and the sunspot area.

The observations of the coronal green line are mainly from the ground-based coronagraphs, except for some limited data from space such as the observations from the Large Angle Spectroscopic Coronagraph (LASCO) C1 instrument on board the SOHO spacecraft (Brueckner et al. 1995; Wang et al. 1997). The LASCO-C1 observed the corona with a field of view extending from 1.1 to 3.0 R_{\odot} using a tunable Fabry–Perot filter, which unfortunately failed to work after the spacecraft freezing (Koutchmy et al. 2005). C1 had provided unprecedented observations in spectral lines since launch in 1995 December until 1998 June. On the other hand, the ground-based coronagraphs are obviously restricted by the night and day alternation, local weather conditions and other unexpected interruptions. Therefore, the fact of very limited coronal stations in the world results in a number of data gaps for the green line observations (Rybanský et al. 2005). Therefore, in order to minimize the “missing” information, the space-based observations might be greatly helpful.

The Atmospheric Imaging Assembly (AIA) on the Solar Dynamics Observatory (SDO) observes the full disk in seven extreme ultraviolet (EUV) channels (Pesnell et al. 2012), where the dominant contributions for six EUV channels are expected by the iron emission lines: 171 Å (Fe IX), 193 Å (Fe XII, Fe XXIV), 211 Å (Fe XIV), 335 Å (Fe XVI), 94 Å (Fe XVIII) and 131 Å (Fe VIII, Fe XX, Fe XXIII). The theoretical study by O’Dwyer et al. (2010) shows that the 211 Å channel has a response at high temperature due to the dominant spectrum

($\log T \sim 6.3$) from Fe XIV, which is suitable for active region observations.

In this paper, we try to reveal the relations between the EUV and the green line intensities for the same coronal features in different scales and at different heliocentric latitudes. In Section 2 we introduce the observations and analysis methods, and in Section 3 we compare the coronal structures between YOGIS and AIA data. Finally, the results and discussion are presented in Section 4.

2. Coronal Data Processing

The Lijiang Coronagraph Station of Yunnan Observatories, established in 2013, was the first optical coronal observation station in China (Liu et al. 2012; Zhao et al. 2018). A 10 cm Lyot coronagraph was shipped from Norikura Station of NAOJ and installed at Lijiang Station during the summer of 2013. The first coronal image was successfully taken on 2013 October 25. The observing system was originally designed by Ichimoto et al. (1999), including a tunable Lyot filter system (with a 1 Å FWHM bandpass, centered at Fe XIV 5303 Å) and a cooled CCD camera (1024 × 1204 pixel array). The system can obtain images with the modes of single-peak, the double-peak, -0.45 and $+0.45$ Å subsequently and repeatedly 8 times to improve the signal-to-noise ratio. Now the 10 cm coronagraph is in well operation in Lijiang, and some sub-systems have been renovated and updated, such as the LCVR control system, the equatorial system, the optical system and the focus control system.

The coronal green line images, taken on 2013 November 10, are used in the present study. The raw data are preprocessed following the standard reduction procedure for calibration. Each frame has been corrected using the corresponding dark and flat fields, and the sky scattered light is subtracted from the continuum intensity. Figure 1 shows one coronal green-line image covering a typical field-of-view (FOV) of $64' \times 64'$ (about 2.0 R_{\odot} in X and Y directions, with a $3''/68$ pixel $^{-1}$ resolution). The minimum coronal height of the inner FOV is 0.03 R_{\odot} from the solar limb. In the left frame of this figure there are two local regions marked “1” and “2” for a relatively small-scale coronal bright structures at latitudes of $S 0^{\circ}$ – 30° at the west limb and a relatively large-scale corona structures across the solar equator at the east limb, respectively. For the coronal loops pattern observed in the regions, we extract their profiles in the plane of the sky (POS) using a loop identification method based on the phase congruency theory (Li et al. 2017). The loop systems are marked by “A” and “B” in the right frame of Figure 1. In the following, each region and loop will be analyzed separately.

To directly assess the relationship between the green line and EUV wavelengths for coronal features, we compare their intensity distributions with simultaneous observations. AIA data can provide full-view of low corona covering at least 1.3

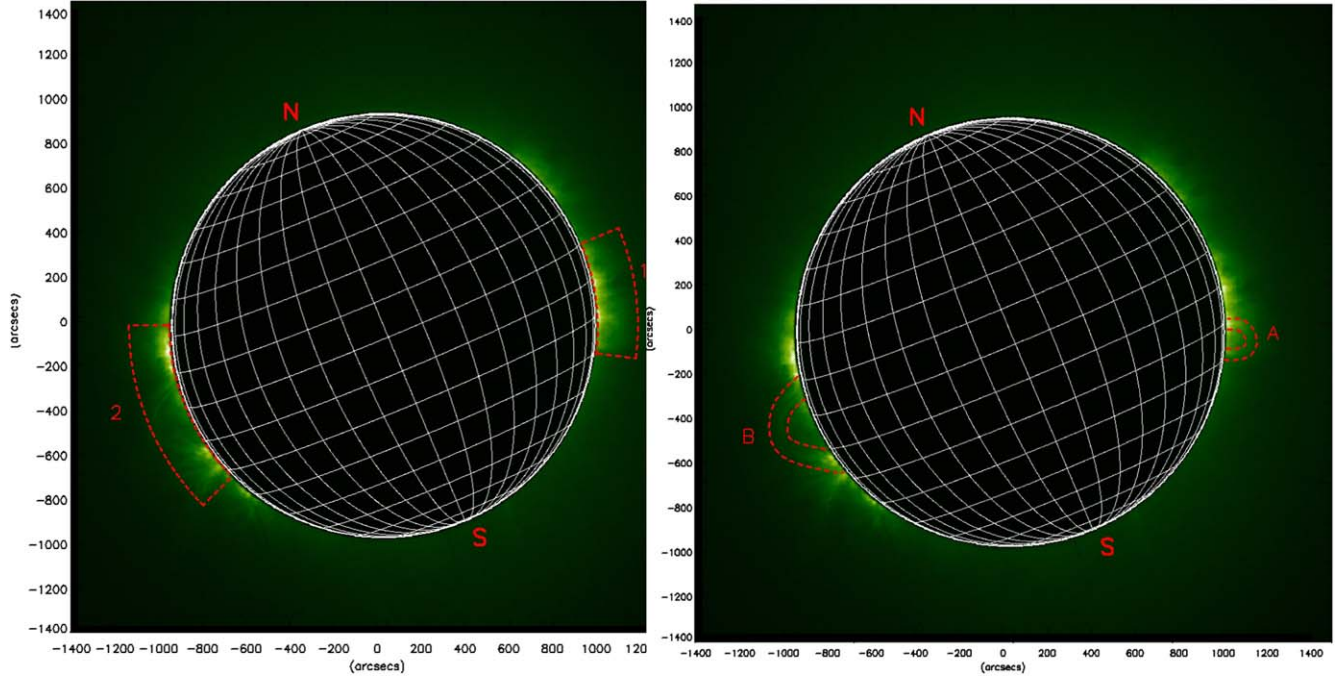


Figure 1. The full FOV observation of YOGIS from Lijiang Station on 2013 November 10 (01:21 UT) for Fe XIV 5303 Å. The half size of the coronagraph occulter is 1.03 solar radii. Two limb regions “1” and “2” (left frame) and two identified coronal loops “A” and “B” (right frame) are chosen for detailed analysis. The arc size of region “1” is 530'' by 180'', and for region “2,” it is 790'' by 180''. The maximum height of the loop “A” is 55'' and the length is about 250'', and for the loop “B,” they are 100'' and 510'', respectively.

solar radii in multiple EUV wavelengths with a high cadence of 12 s and a $0''.6 \text{ pixel}^{-1}$ resolution (Lemen et al. 2012). Before the intensity comparison, the positional alignment for two images from YOGIS and AIA needs to be made. First, the AIA image spatial resolution is adjusted to be the same as the lower resolution of the YOGIS data ($3''.7 \text{ pixel}^{-1}$) by shrinking the data size. Second, the coordinate directions of the AIA image are also rotated to fit that of the YOGIS data by correcting the p-angle. Third, we overlap the two images and check the spatial deviation between the identical loop features in the green line and EUV images. Finally, we manually align the EUV image by shifting it in X and Y directions until the best shifting concordance is achieved for the loops in the two wavelengths to overlap well with each other. The alignment precision is thought to be consistent with the YOGIS data resolution, which is enough for the analysis of the large-scale loops selected in this paper. After the careful image alignment, rotation and resolution correcting, the green line signals match well with the EUV bright features. Figure 2 shows the composite coronal images, in which the SDO/AIA data have been zoomed out just for better visual comparison of the bright coronal structures with the green line data. It is obvious that there exists a generally good correspondence between the loops for each composite image. It should be noted that the structural similarity of coronal observations can only be used as a

reference for correlation, while the strict comparison of point-to-point by pixels remains the key to an adequate correlation analysis.

For the analysis of the correlation coefficient distribution within the selected regions, we use two different algorithms shown in “Pattern A” and “Pattern B” in Figure 3 to analyze the distribution along the directions of the position angle (PA) and the heliocentric height increase, respectively. For “Pattern A,” the correlation coefficient at every y (along the PA direction) is calculated within the corresponding vertical strip (blue rectangular region), and for “Pattern B,” the correlation coefficient at every x (along the height increasing direction) is calculated within the corresponding parallel strip (blue concentric circular region).

3. Correlations of Coronal Structures

All the EUV channels of AIA are used to analyze the EUV intensity correlations with the coronal green line. Figure 4 shows the distribution of the correlation coefficients in region “1” along the Y-axis direction according to the “Pattern A” algorithm. Note that in order to obtain enough sample points for each vertical strip, data interpolation is used. In the calculations, the points in X/Y direction are set to be 100/600, respectively. “Coff (mean)” represents the average correlation coefficient along Y. The top-left panel of Figure 4 highlights the

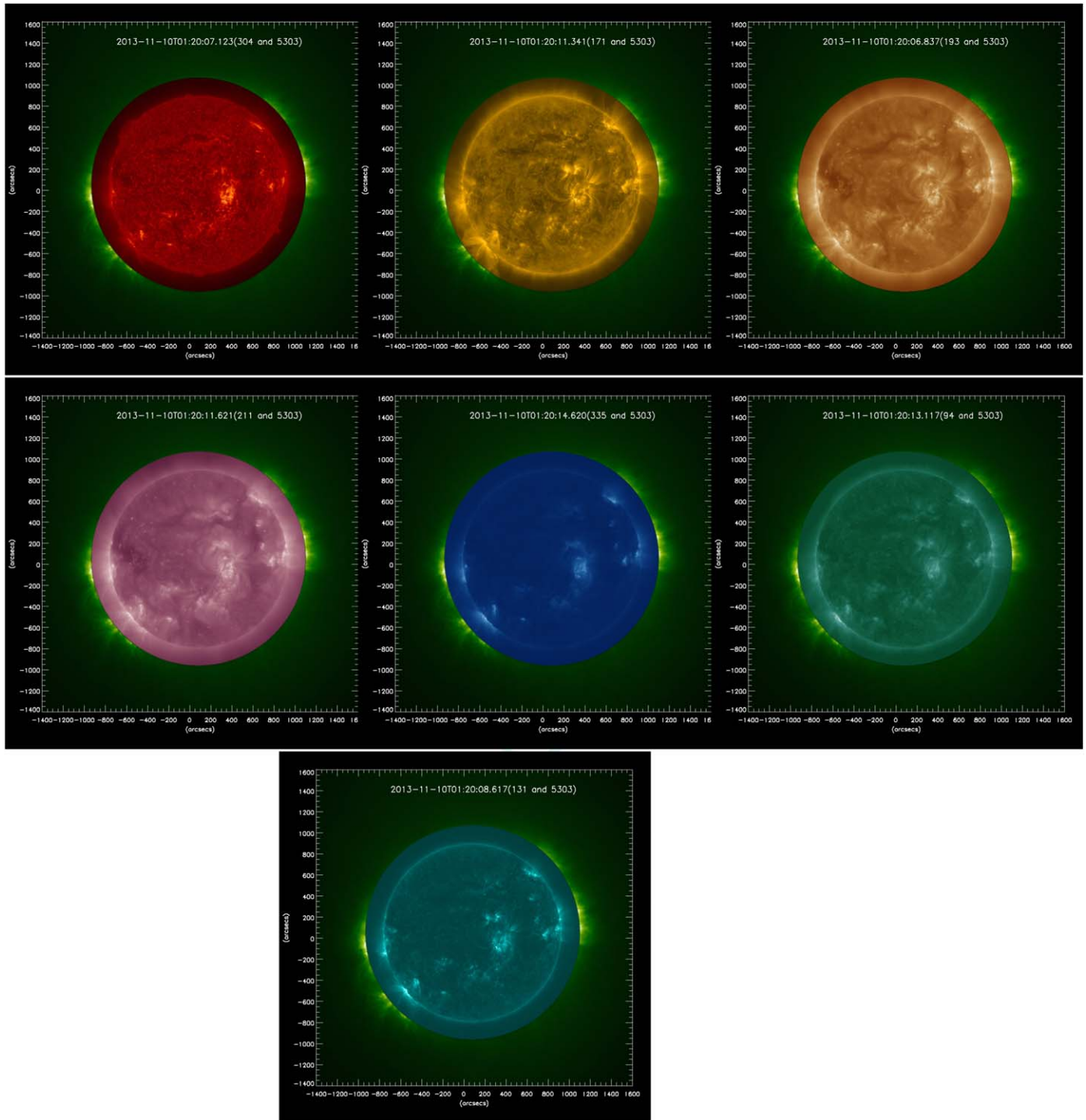


Figure 2. Composite coronal images from the green line data and the EUV data, which are 304, 171, 193, 211, 335, 94 and 131 Å from the first frame to the last one. All these images are shown without any enhancement.

median intensity profiles for every wavelength with different colors. The other panels display the high average correlations (ranged from 0.95 to 0.99) for every pair of wavelengths. It can be seen that the coronal green line and the EUV wavelengths

have very similar tendency of intensity profiles along the Y direction except for the obvious deviation for 171 Å between $y = 0.2$ and $y = 0.5$. The highest correlation coefficient of 0.99 is only found between the line pair of 5303 and 211 Å.

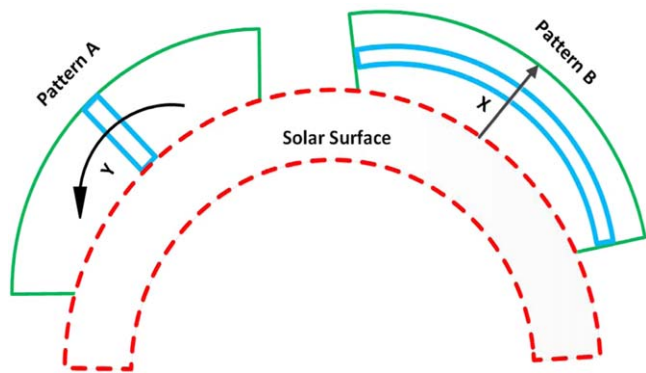


Figure 3. Showing two algorithms for extracting coronal intensity distributions. “Pattern A” means to obtain the distribution of the correlation coefficients along the Y -axis direction, i.e., the position angle increasing direction. “Pattern B,” along the X -axis direction, i.e., the height increasing direction.

Figure 5 reports the results of correlation coefficients along the X direction within region “1” using the “Pattern B” algorithm. As can be seen from the figure, all these coronal intensities are decreasing with height while the differences among them are also all getting smaller. The intensity correlation coefficients are found lower for the three EUV lines of 131 Å, 94 Å and 171 Å, being 0.53, 0.49 and 0.2, respectively, while it is the highest value of 0.89 for between 5303 and 211 Å.

Figures 6 and 7 illustrate respectively the correlation for region “2” between the green line and the AIA EUV intensity data according to the algorithms of “Pattern A” and “Pattern B.” Region “2” is larger and it contains most of the visible structures on the east limb. The calculations for region “2” is similar to region “1.” Figure 6 shows that the correlation coefficients vary significantly along the PA direction, and the “Coff (mean)” values are still all greater than 0.9. Interestingly, the correlation coefficient between 5303 and 211 Å is also the strongest (0.97), and it is also the lowest for the pair of 5303 and 171 Å (0.91). For Figure 7, it can also be seen that all the coronal intensities decrease with the heliocentric height. The “Coff (mean)” value for the pair of 5303 and 211 Å lines is much higher than those of the other line pairs, being the lowest for 171 Å. The other lower values are found for 94, 131 and 193 Å lines, very similar to the results from region “1.”

Several loop systems can be distinguished at different scales above the east and west limbs in the coronal green line images. In order to compare the intensities of the loops appeared in the green and the EUV lines more clearly, in Figures 8 and 10 the same algorithm of “Pattern A” is used to analyze the smaller loop “A” and the larger loop “B.” In the calculations, the points in X/Y direction are set to be 100/300, respectively. The top-left panels in Figures 8 and 10 show the distribution of the coronal intensities along the Y direction which are plotted with different colored lines. It is unsurprised to find that the coronal

intensities along a loop system usually show the same decrease tendency from one footpoint toward the loop top, and then exhibit the same increase tendency from the top toward the opposite footpoint. Again, it is interesting to obtain the similar results, i.e., the pair of lines of 5303 and 211 Å still have the highest correlation coefficient 0.93 for loop systems. Figures 9 and 11 illustrate the correlation coefficient distributions for every wavelength along the X direction, and the highest correlation is still found for between 5303 and 211 Å lines. Such a strong correlation between 5303 and 211 Å emissions, consistent for both coronal loops and large regions at different limb locations, had never been reported before.

4. Discussion and Conclusions

The inner corona can be well observed by the green line from ground-based coronagraphs and by the EUV wavelengths from space telescopes, however, the detailed relation between them is not very clear until now mainly due to the shortage of the two-dimensional green-line data and the limited bands ever used for the EUV observations. For example, to improve the green-line coronal index (CI) quality, Lukáč & Rybanský (2010) compared CI with the EUV measurements on the CELIAS/SEM equipment by choosing the flux within the bandpass 260–340 Å because of no other better choices were available. Since the launch of SDO, several new EUV wavelengths have been used for high-resolution images supplied, including the 211 Å channel, which was not utilized by TRACE, SOHO and STEREO for two-dimensional full-disk imaging before.

In this paper, we present the fresh results by comparing the coronal intensities between the coronal green line and every channel of AIA EUV observations. Before the comparison, the data from YOGIS and AIA have been adjusted for the spatial resolution uniformity, solar center alignment, p -angle correction, data interpolation and brightness calibration through standard procedures. Two typical coronal regions and two loop systems above the solar west and east limbs are studied for comparing the intensity distributions extracted by two different algorithms. The main results are summarized as follows:

1. Along the increase directions of height and PA, for the two limb coronal regions, the lines pair of 5303 and 211 Å always keep the highest intensity correlation based on two algorithms. The coefficients range from 0.86 to 0.99.
2. Along the increase directions of height and PA, for the cross-sections in two typical loop systems, it is the same to find the strongest correlation for the intensity distributions of the two lines 5303 and 211 Å, consistent with the previous conclusion.
3. For six cases among the total eight calculation results shown in Figures 4–11, the correlation coefficients are found to be the relatively lowest for the lines pair of 5303

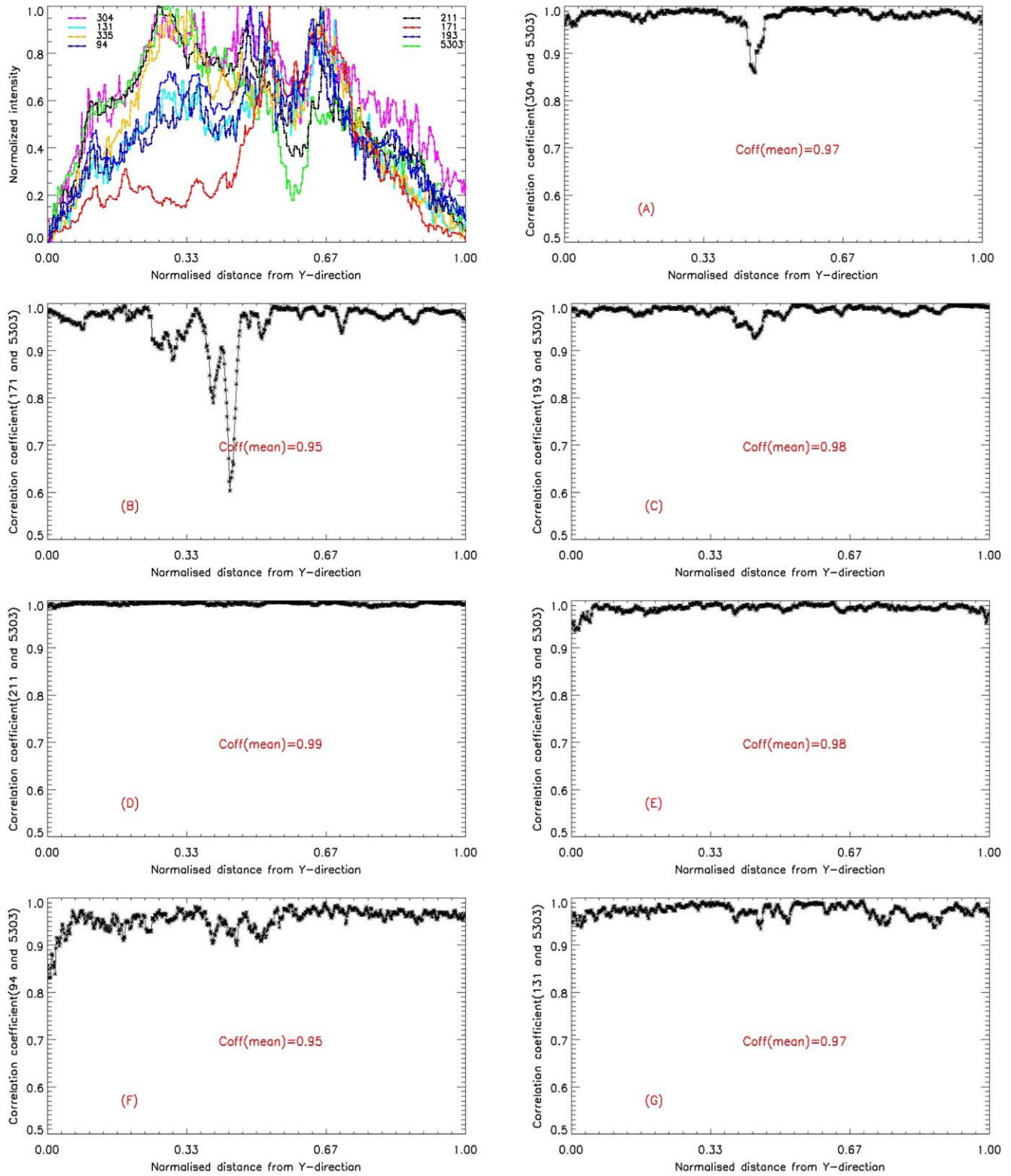


Figure 4. Profiles of the coronal green line and EUV intensities, and their correlation coefficients by “Pattern A” algorithm for region “1.” The first frame shows the median values of coronal green line and EUV wavelengths within each vertical strip (blue region) along Y (Figure 3), respectively. Panels (A) to (G) represent the correlation coefficients distribution of the coronal green line intensity with each of EUV wavelengths, which are 304, 171, 193, 211, 335, 94, and 131 Å. “Coff(mean)” represents the average of the correlation coefficients.

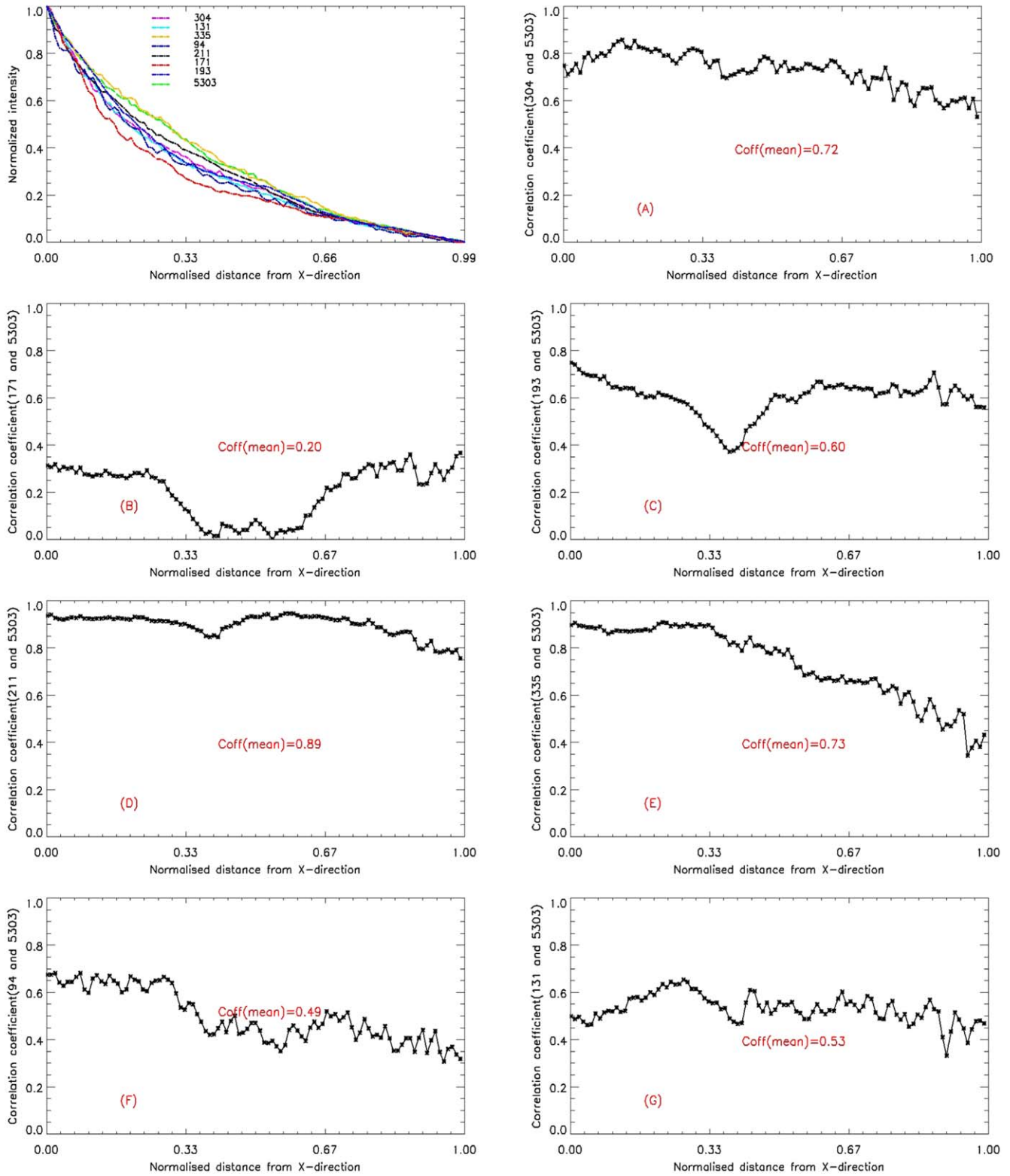


Figure 5. Same as Figure 4, while using “Pattern B” algorithm for region “1.”

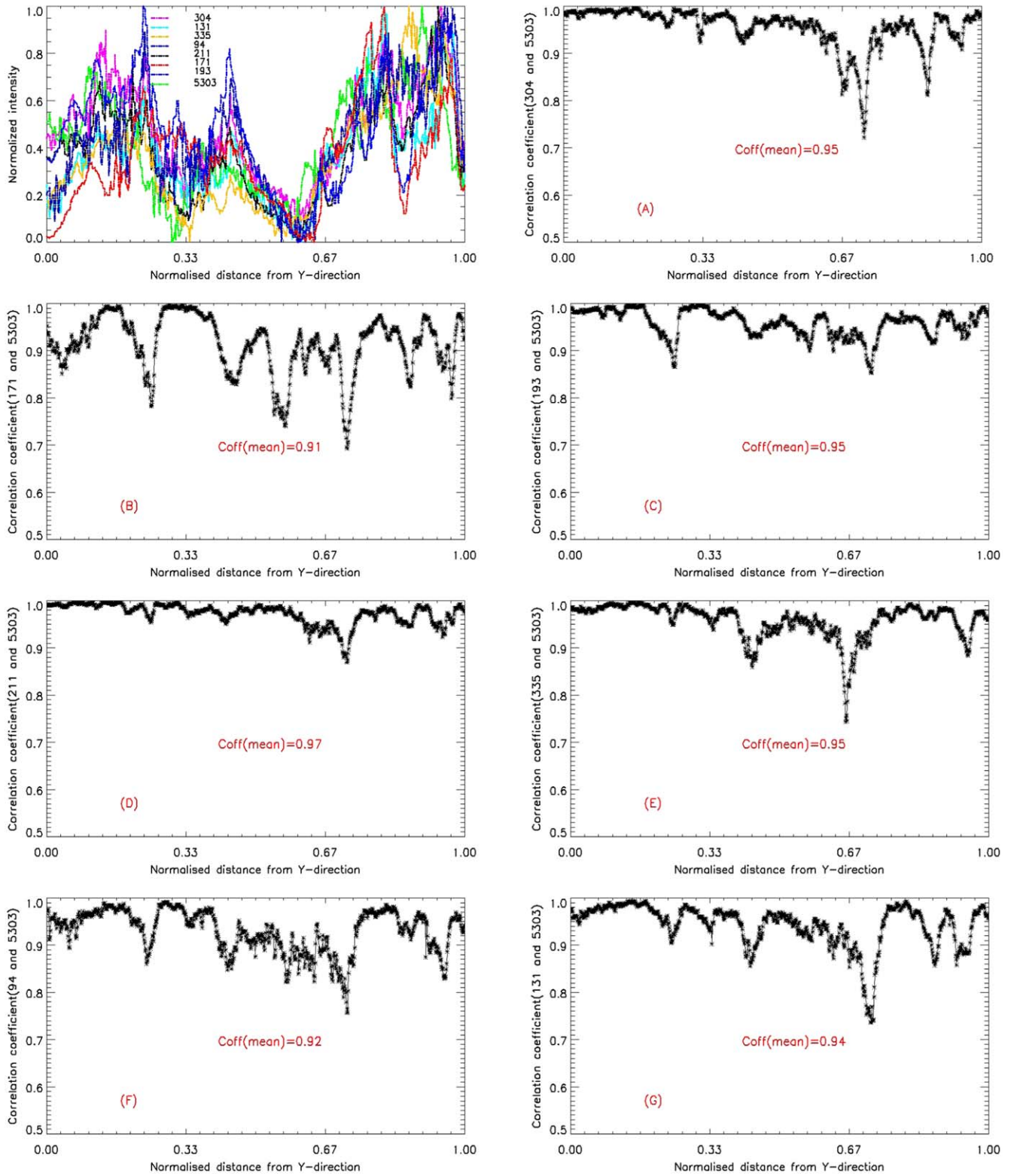


Figure 6. Same as Figure 4, while using “Pattern A” algorithm for region “2.”

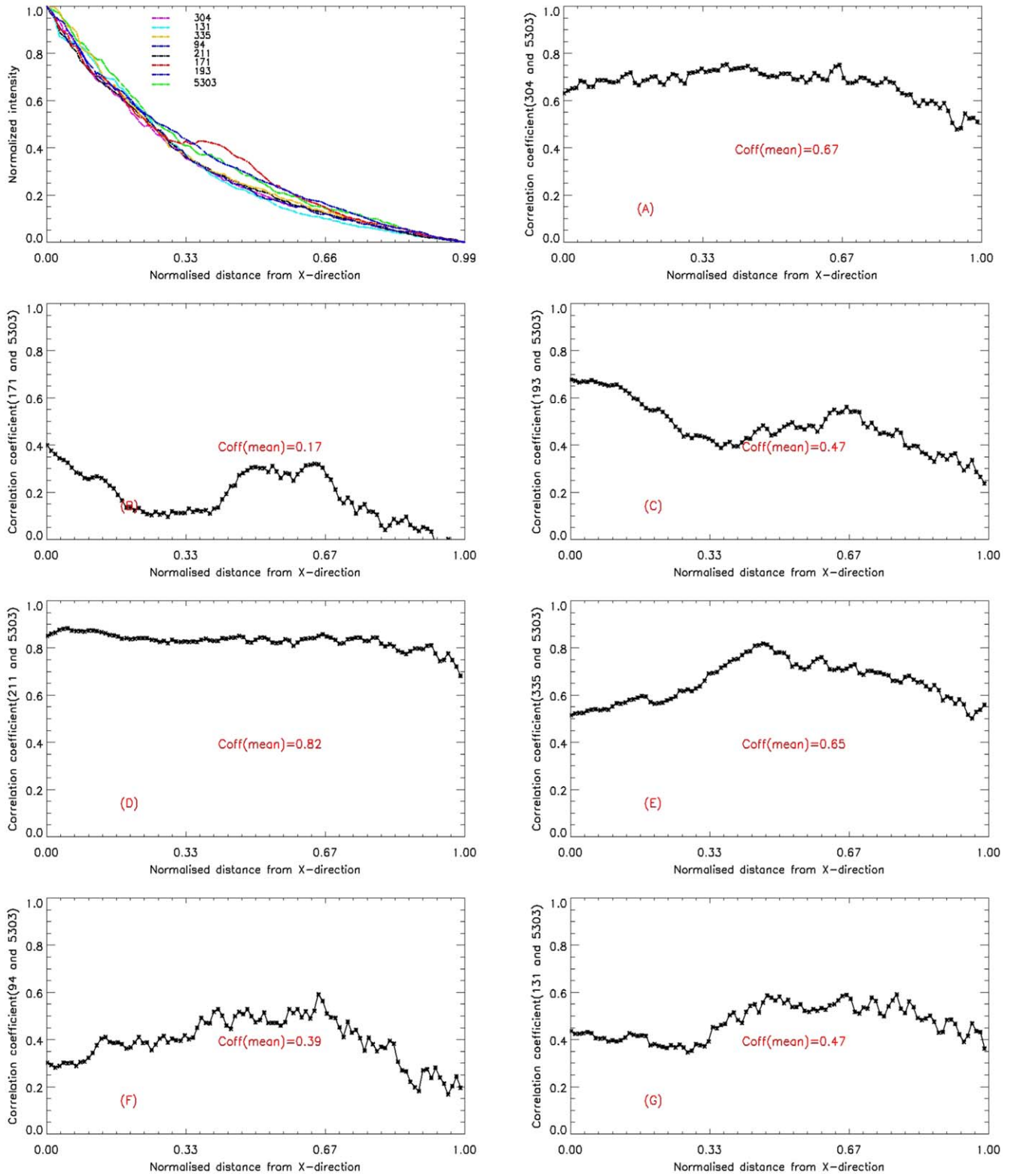


Figure 7. Same as Figure 4, while using “Pattern B” algorithm for region “2.”

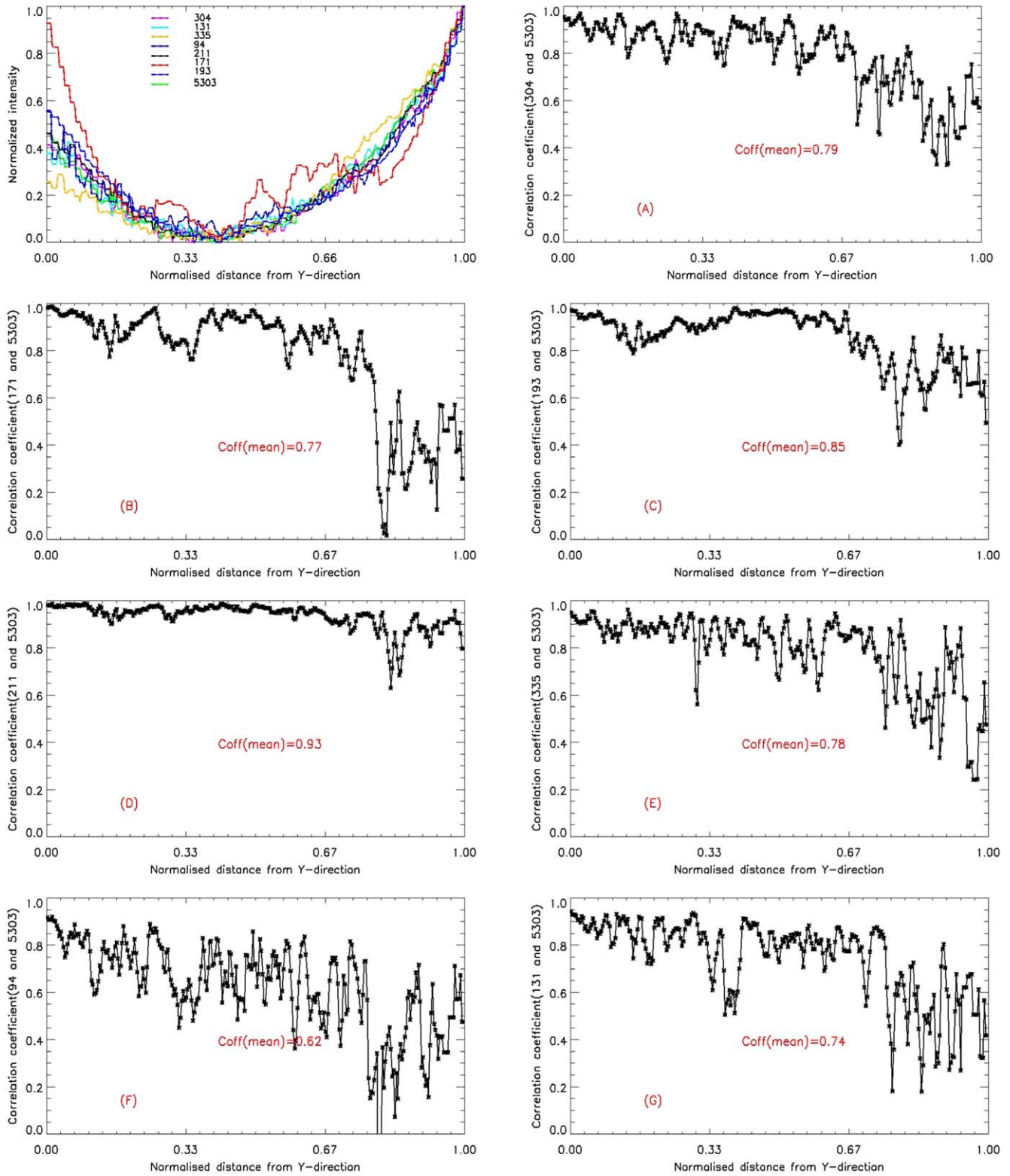


Figure 8. Same as Figure 4, while using “Pattern A” algorithm for loop “A.”

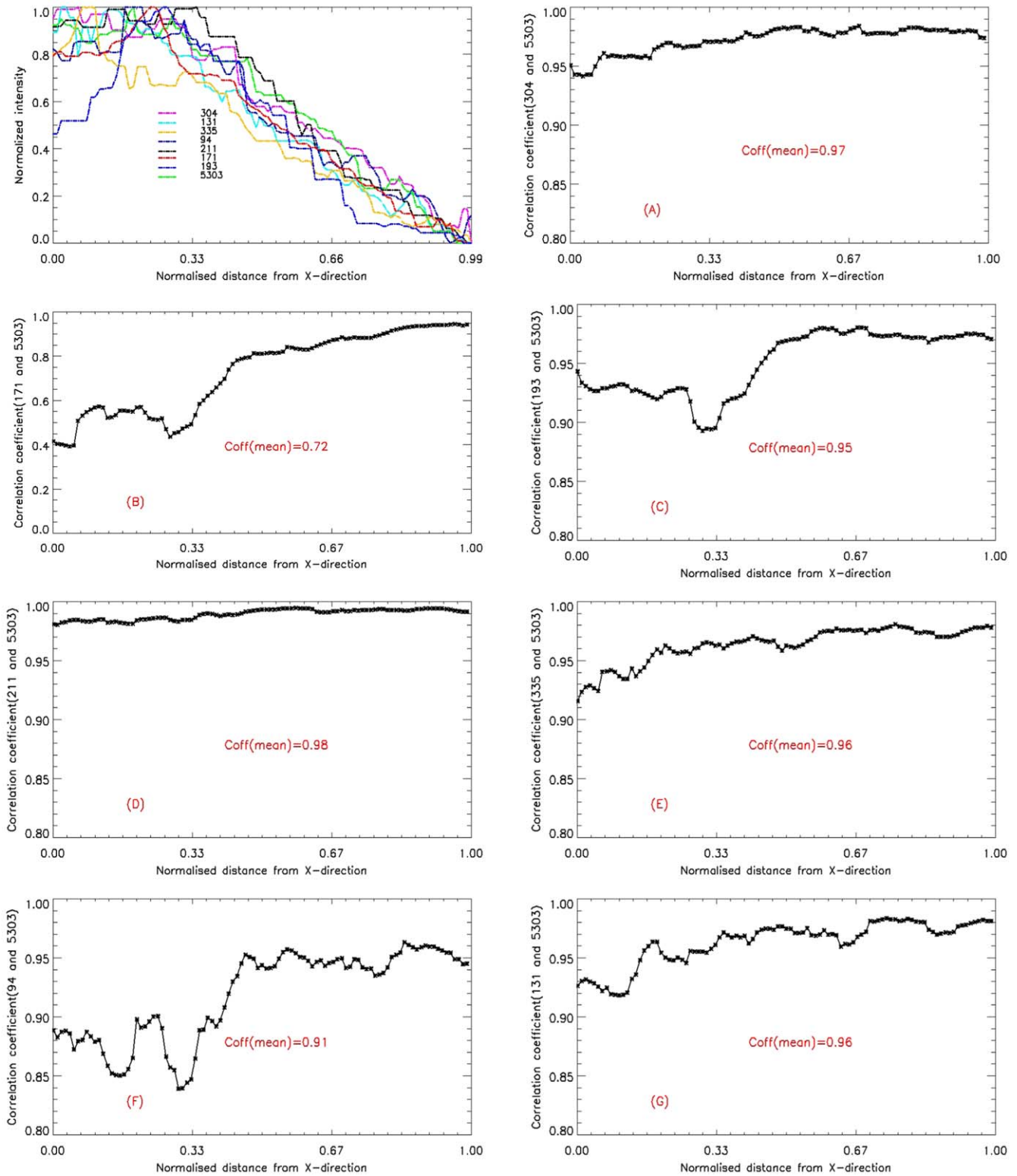


Figure 9. Same as Figure 4, while using “Pattern B” algorithm for loop “A.”

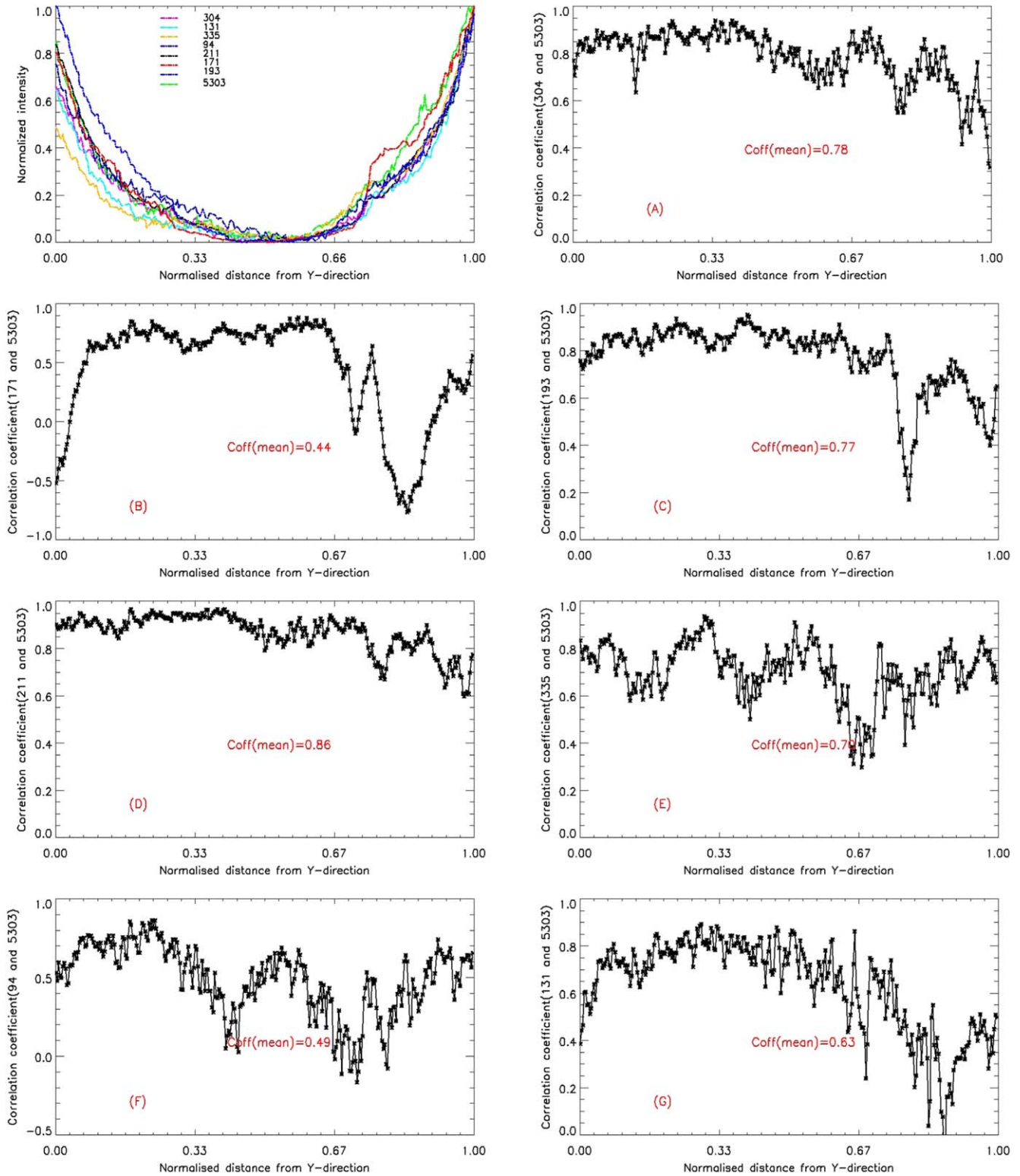


Figure 10. Same as Figure 4, while using “Pattern A” algorithm for loop “B.”

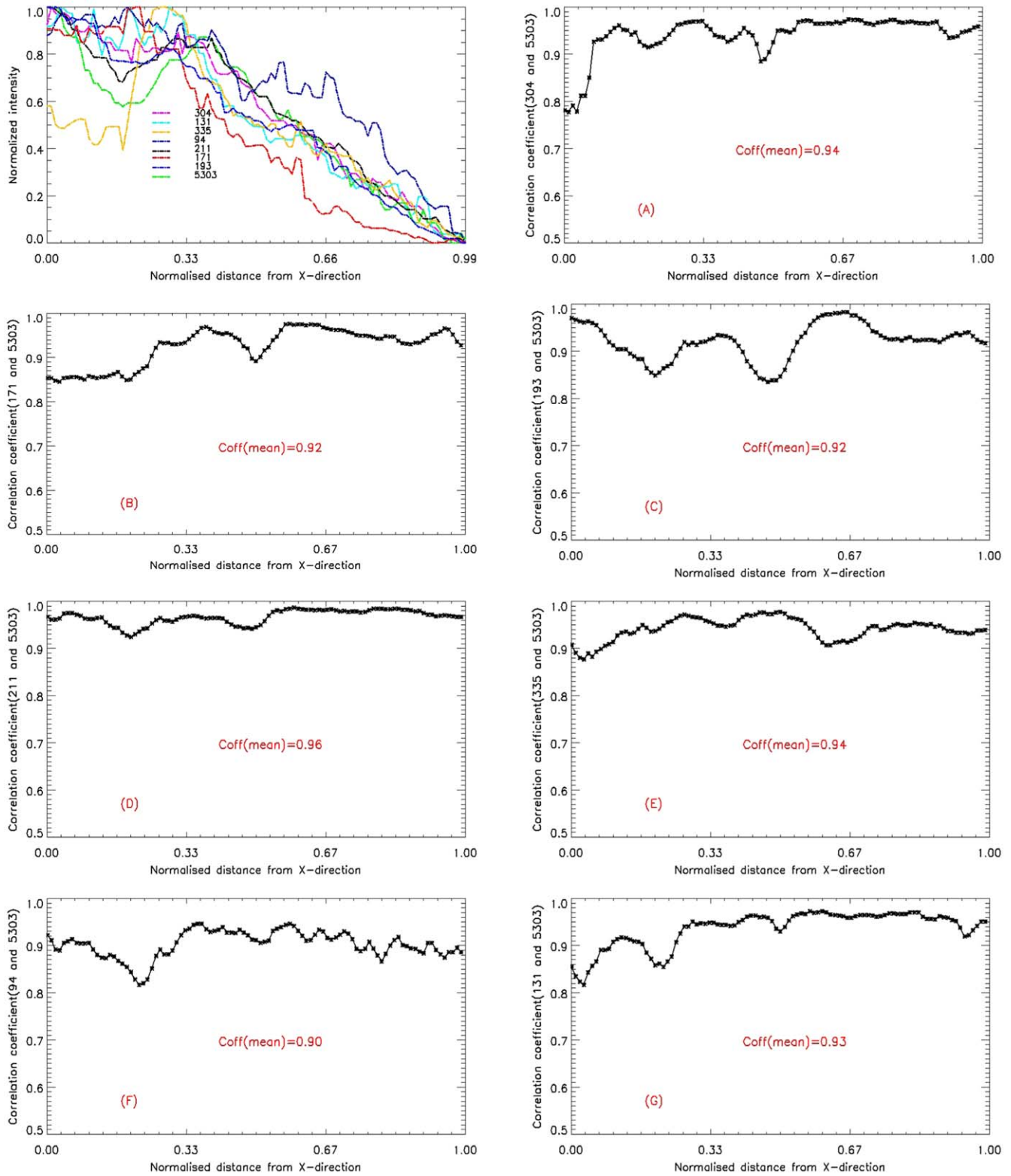


Figure 11. Same as Figure 4, while using “Pattern B” algorithm for loop “B.”

and 171 Å. These lowest coefficients range from 0.17 to 0.95.

The main reason for the low correlation between 5303 and 171 Å may be due to the fact that the dominant emission (80%) of the 171 Å line originated from active region is contributed by ion Fe IX whose temperature of maximum abundance is less than 1 MK, half cooler than that of the 5303 Å line. On the contrary, the dominant (39%) emission of 211 Å from active region is contributed by the same ion Fe XIV as 5303 Å, which can render the higher correlation between the green line and the 211 Å line than the other pairs. However, it is unclear why the correlation between the hot line emission of Fe XIV 5303 Å and the cool line emission of He II 304 Å seems not bad in our study, with the coefficients ranging from 0.72 to 0.97. This might be explained to be due to the cool He II plasma injection from the chromosphere into the same coronal magnetic field structures as the Fe XIV emissions illustrated with the low spatial resolution in our work. Liu (2009) studied the spatial correlation between bright loop features in EUV (171 and 195 Å) and the inferred NIR (10747 Å) emission sources, finding that the relative locations of the NIR emission sources to that of the bright EUV loops were highly correlated with the intensity of the magnetic fields in large scale.

On the other hand, the results of our present study can help to connect the physical processes observed in different heights in the corona by precisely tracking the bright loops or other features observed in 5303 Å above the limb down to the correct surface locations revealed by the 211 Å data. Moreover, the ground-based observations of the coronal green line are usually limited by the night and day alternation, local weather conditions and other complicated factors, that can easily cause discontinuity for observations and unclear errors for data analysis, such as the complicated coronal index calculations. Due to the LASCO-C1's Fabry–Perot filter work failure since 1998, there has been no coronal green line observations available from space until now. The AIA 211 Å observations, together with the other EUV data taken successively from space, are very encouraging to fill in the “missing” observational gaps for the green line data, which is important for the long-term study of solar cycles.

Finally, we must admit that due to the small aperture of the Lijiang coronagraph, some conclusions made in this work are very preliminary and need to be further confirmed and improved by future higher-resolution observations for corona. Therefore, the development of the next-generation instruments, such as the large coronagraph of 1 m aperture in the project of CGST (Chinese Giant Solar Telescope) (Fang 2011; Liu 2014; Deng et al. 2016; Liu et al. 2016, 2021) and the space coronagraph of ASPIICS (Association of Spacecraft for Polarimetric and Imaging Investigation of the Corona of the Sun) (Bemporad et al. 2017), are highly awaited in this rapidly developing area.

Acknowledgments

We sincerely thank the SDO team for the use of their observations; we also thank Prof. T. Sakurai-san and the NAOJ team for the 10 cm coronagraph collaboration. This work is supported by the National Natural Science Foundation of China under grants (11873090, 12173086, 11903016, 11533009, 11873092, U2031148 and U1931116) and the Light of West China program of CAS. The authors extend their appreciation to the Deanship of Scientific Research at King Saud University for funding this work through research group No. (RG-1440-092). We acknowledge for the data resources from the National Space Science Data Center, National Science & Technology Infrastructure of China (<http://www.nssdc.ac.cn>).

ORCID iDs

Fei-Yang Sha,  <https://orcid.org/0000-0002-2995-070X>

References

- Antonucci, E., Harra, L., Susino, R., & Telloni, D. 2020, *SSRv*, **216**, 117
- Arnaud, J. 1982, *A&A*, **112**, 350
- Bemporad, A., Pagano, P., Giordano, S., & Fineschi, S. 2017, *ExA*, **44**, 83
- Brueckner, G. E., Howard, R. A., Koomen, M. J., et al. 1995, *SoPh*, **162**, 357
- Dai, J., Ji, H., Li, L., Zhang, J., & Chen, H. 2021, *ApJ*, **906**, 66
- Deng, L. H., Qu, Z. Q., Wang, K. R., & Li, X. B. 2012, *AdSpR*, **50**, 1425
- Deng, Y., Liu, Z., Qu, Z., Liu, Y., & Ji, H. 2016, in *ASP Conf. Ser.* 504, *Coimbra Solar Physics Meeting: Ground-based Solar Observations in the Space Instrumentation Era*, ed. I. Dorotovic, C. E. Fischer, & M. Temmer (San Francisco, CA: ASP), 293
- Doschek, G. A., Feldman, U., Laming, J. M., Schühle, U., & Wilhelm, K. 2001, *ApJ*, **546**, 559
- Edlén, B., & Swings, P. 1942, *ApJ*, **95**, 532
- Fang, C. 2011, *RAA*, **11**, 1377
- Gnevyshev, M. N., Nikolsky, G. M., & Sazanov, A. A. 1967, *SoPh*, **2**, 223
- Grotian, W. 1934, *ZAp*, **8**, 124
- Guhathakurta, M., & Fisher, R. R. 1994, *SoPh*, **152**, 181
- Ichimoto, K., Noguchi, M., Tanaka, N., et al. 1999, *PASJ*, **51**, 383
- Ji, H., Cao, W., & Goode, P. R. 2012, *ApJL*, **750**, L25
- Ji, H., Hashim, P., Hong, Z., et al. 2021, *RAA*, **21**, 179
- Koutchmy, S., Contesse, L., Viladrich, C., Vilinga, J., & Bocchialini, K. 2005, in *ESA Special Publication, Vol. 11, The Dynamic Sun: Challenges for Theory and Observations (Leuven)* ed. D. Danesy et al., 26.1
- Lemen, J. R., Title, A. M., Akin, D. J., et al. 2012, *SoPh*, **275**, 17
- Li, H., Zhao, M., & Liu, Y. 2017, *ChA&A*, **41**, 357
- Liu, Y. 2009, *AnGeo*, **27**, 2771
- Liu, Y., Shen, Y. D., Zhang, X. F., & Liu, N. P. 2012, *SoPh*, **279**, 561
- Liu, Y., Song, T., Zhang, X., et al. 2016, in *Solar and Stellar Flares and their Effects on Planets*, ed. A. G. Kosovichev, S. L. Hawley, & P. Heinzel, Vol. 320 (Cambridge: Cambridge Univ. Press), 447
- Liu, Y., & Zhang, X. 2018, The coronal green line monitoring: a traditional but powerful tool for coronal physics, in *Long-Term Datasets for the Understanding of Solar and Stellar Magnetic Cycles*, *Proc. IAU Symp.* No. 340, ed. D Banerjee (Jaipur, India) 169
- Liu, Y., Zhang, X., Song, T., et al. 2021, *Proc. SPIE*, **12070**, 120700B
- Liu, Z. 2014, in *ASP Conf. Ser.* 489, *Solar Polarization 7*, ed. K. N. Nagendra et al., 247
- Lukáč, B., & Rybanský, M. 2010, *SoPh*, **263**, 43
- Lytot, B. 1939, *MNRAS*, **99**, 580
- Makarov, V. I., Tlatov, A. G., & Callebaut, D. K. 2003, in *ESA Special Publication, Vol. 535, Solar Variability as an Input to the Earth's Environment (Tatranská)* ed. A. Wilson, 217
- Minarovech, M., Rušin, V., Rybanský, M., Sakurai, T., & Ichimoto, K. 2003, *SoPh*, **213**, 269

- O'Dwyer, B., Del Zanna, G., Mason, H. E., Weber, M. A., & Tripathi, D. 2010, *A&A*, **521**, A21
- Pesnell, W. D., Thompson, B. J., & Chamberlin, P. C. 2012, *SoPh*, **275**, 3
- Petrovay, K., Nagy, M., Gerják, T., & Juhász, L. 2018, *JASTP*, **176**, 15
- Raju, K. P., Chandrasekhar, T., & Ashok, N. M. 2011, *ApJ*, **736**, 164
- Ramesh, K. B., Nagabhushana, B. S., & Varghese, B. A. 1999, *SoPh*, **188**, 99
- Rybanský, M., Rušin, V., Minarovjech, M., Klocok, L., & Cliver, E. W. 2005, *JGRA*, **110**, A08106
- Sakurai, T. 2012, in ASP Conf. Ser. 454, *Hinode-3: The 3rd Hinode Science Meeting*, ed. T. Sekii, T. Watanabe, & T. Sakurai (San Francisco, CA: ASP), 439
- Sakurai, T., Ichimoto, K., Raju, K. P., & Singh, J. 2002, *SoPh*, **209**, 265
- Sakurai, T., Rusin, V., & Minarovjech, M. 2004, *AdSpR*, **34**, 297
- Shen, Y., & Liu, Y. 2012, *ApJ*, **754**, 7
- Smartt, R. N., Zhang, Z., & Smutko, M. F. 1993, *SoPh*, **148**, 139
- Srivastava, A. K., Singh, J., Dwivedi, B. N., et al. 2007, *BASI*, **35**, 457
- Stix, M. 2004, *The Sun: An Introduction* (Berlin: Springer)
- Sýkora, J. 1969, *BAICz*, **20**, 70
- Tian, H., McIntosh, S. W., Wang, T., et al. 2012, *ApJ*, **759**, 144
- Wang, Y. M., Sheeley, N. R. J., Hawley, S. H., et al. 1997, *ApJ*, **485**, 419
- Wood, B. E., Karovska, M., Cook, J. W., et al. 1998, *ApJ*, **505**, 432
- Yang, X., Ji, H.-s., & Li, H.-C. 2015, *ChA&A*, **39**, 66
- Young, C. A. 1870, *Natur*, **1**, 532
- Zhang, X., Liu, Y., Zhao, M., et al. 2022, *RAA*, **22**, 075007
- Zhao, M. Y., Liu, Y., Elmhamdi, A., et al. 2018, *SoPh*, **293**, 1